Optical phonons of alternating chains with $\frac{3}{4}$-filled bands and internal degrees of freedom: A simple model for Ca_2CuO_3

S.-L. Drechsler and J. Malek*
Institut für Festkörper- und Werkstofforschung Dresden e.V., Postfach, D-01171 Dresden, Germany

M. Yu. Lavrentiev† and H. Köppel
Physikalisch-Chemisches Institut der Universität Heidelberg, Im Neuenheimer Feld 253, D-69120 Heidelberg, Germany
(Received 5 April 1993; revised manuscript received 13 September 1993)

The long-wavelength phonon spectrum of an alternating chain, consisting of molecules with internal degrees of freedom and ions (atoms) in between, is investigated within a frozen-phonon-type approach for the period-4 mixed charge-density-wave–bond-order-wave (CDW-BOW) ground state of an one-dimensional Hamiltonian with $\frac{3}{4}$-filled bands, diagonal, and off-diagonal electron-phonon interaction. Raman and infrared data of the recently synthesized quasi-one-dimensional system $Ca_{1.8}Sr_{0.2}CuO_3$ are analyzed within this model. The occurrence of "forbidden" Raman modes is explained semiquantitatively as the consequence of the period-4 CDW-BOW ground state. The parameters derived from the experimental data are consistent with intermediately strong electron-electron interaction. Necessary experiments to check the relevance of the proposed model are discussed.

I. INTRODUCTION

There is a continuing interest in the study of quasi-one-dimensional systems with variable chemical complexity. A large number of papers has been devoted to polyenes and transition-metal halogen-bridged (MX-chain) compounds (see, e.g., Refs. 1–5). Dynamical properties of the commensurate charge-density-wave (CDW) and/or bond-order-wave (BOW) states of one-dimensional Peierls systems with more than one degree of freedom have been reported for the half-filled band case (period 2) by Rice[6] for charge-transfer salts and by Horovitz[7] for polyacetylene. The paper of Rice and Mele[8] contains also a microscopic consideration of the dynamics of period-2 alternating chains, but without internal modes. Some aspects of the dynamics of period-4 alternating chains with applications to MX chains have been discussed microscopically[2] and phenomenologically.[3,4] In Ref. 4 symmetric ligand vibrations have been considered also.

Another interesting class of materials which has attracted less attention so far are the metal-*oxygen*-bridged chains present in some high-T_c superconductors (HTSC's) and related compounds, e.g., the CuO_3 chains in the well-known $YBa_2Cu_3O_7$ system or the recently synthesized $Ca_{2-x}Sr_xCuO_3$ compound.[9] According to local-density-approximation (LDA) band-structure calculations carried out for $YBa_2Cu_3O_7$,[10] there is a partially filled quasi-one-dimensional (1D) band arising from these chains. It is noteworthy that the electronic structure near the Fermi level and the electron-lattice interaction of metal-oxygen-bridged chains seem to be essentially affected by the side groups attached to the metal ion.[11]

The charge per CuO_3 unit in Ca_2CuO_3 is -4, and the corresponding highest occupied band is half-filled (see also the Appendix). Within a simple tight-binding approach these chains can be modeled by a two-band Hamiltonian using the antibonding orbitals of the $Cu(1)O(4)_2$ "molecules" (A sites) and the p_y orbital of the bridging oxygen O(1) (B sites), where the site notation of $YBa_2Cu_3O_7$ has been adopted. [Notice the different notations in Ref. 9 used for the description of $Ca_{1.8}Sr_{0.2}CuO_3$: "O(1)" for the "apical" ("axial") oxygen and "O(2)" for the bridging oxygen.] In the corresponding two-band model the band filling ratio is 3/4. The corresponding Raman active totally symmetric Cu-O(4) stretching mode can be regarded as an internal mode strongly coupled to the chain electrons. The in-chain vibrations giving rise to modulations of the transfer integral between A and B sites seem to be important, too. The model Hamiltonian for CuO_3 chains proposed recently[12] contains also further, partially competing, terms of these two modes. We report here as a first step on dynamical properties of a reduced Hamiltonian containing only four electronic parameters (instead of eight parameters) but having the same symmetry of the CDW ground state, first considered in Ref. 13. Therefore, the Hamiltonian parameters should be considered as effective ones.

Applying this Hamiltonian to Ca_2CuO_3, we yield the ground state with a period-4 superstructure which should be observed experimentally. We have also investigated the reduced Hamiltonian with respect to nonlinear excitations.[14] A rich variety of polaronic and solitonic excitations has been found.

Thus, the aim of the present paper is twofold: (i) to continue the systematical study of that reduced Hamiltonian, to deduce information from the analysis of the phonon spectrum on the chain ground state, and (ii) to contribute to the clarification of the role of the electron-lattice interaction in Cu-O systems.

The paper is organized as follows. In Sec. II the Hamil-

tonian and the method used to calculate phonons are described. Results obtained for a parameter set similar to the set used for $YBa_2Cu_3O_7$ (Ref. 12) are reported in Sec. III. A critical comparison with experimental data of $Ca_{2-x}Sr_xCuO_3$ is given, too. In Sec. IV, based on a brief consideration of the electronic structure of CuO_2 molecules given in the Appendix, we propose a simple scenario to illustrate why the electron-electron correlation effects might be somewhat suppressed and why an effective one-particle two-band Hamiltonian can be applied to Ca_2CuO_3.

II. THE MODEL AND THE METHOD

A schematic view of a single CuO_3 chain, its lattice, and internal coordinates as well as the ground state superstructure (for $\frac{3}{4}$-filled bands) are shown in Fig. 1.

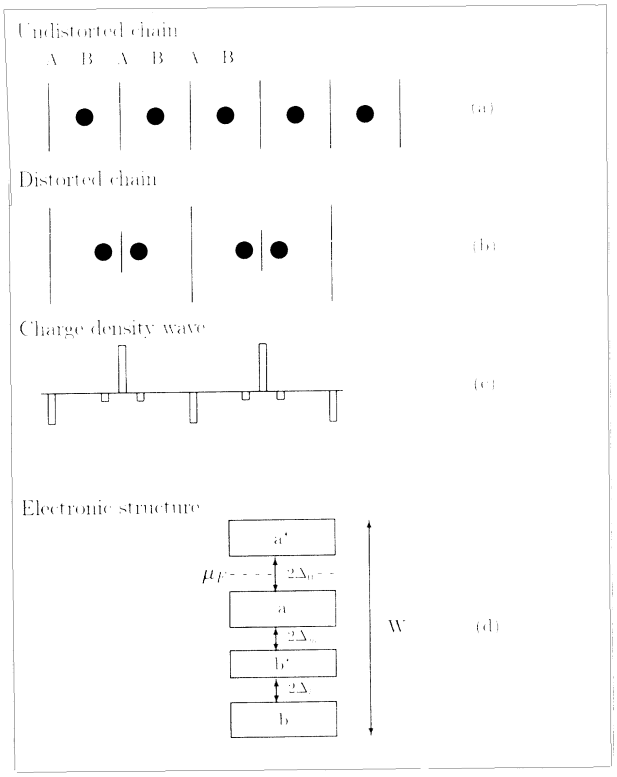

FIG. 1. Superstructure and electronic structure for $\frac{3}{4}$-filled bands. Schematical view of the structure (a) of the metallic equidistant undistorted chain with uniform molecules (A sites) and atoms (B sites) in between, (b) of the distorted insulating chain with enlarged and shortened molecules and pairwise displaced atomic sites, (c) of the charge density wave [in units of $|e|$ the maximal charge density is 0.69 for parameter set I (see text and Table I)], and (d) of the band structure. Here $2\Delta_0 = 2.12$ eV denotes the upper Peierls gap and $2\Delta_l = 1.48$ eV is the lower Peierls gap [see Eq. (A6)]. The middle gap $2\Delta_m = 0.98$ eV stems mainly from the electronic heterogeneity $\Delta\varepsilon = 1.23$ eV between A and B sites. $W = 6.33$ eV denotes the total bandwidth. The Fermi level is given by μ_F [Eq. (A7)]; i.e., bands b, b^*, and a are occupied, whereas a^* is empty.

The chain is oriented along the $y(b)$ axis and the CuO_2 molecules are directed along the $z(c)$ axis (see Fig. 2). The adopted Hamiltonian[13] reads

$$H = H_{\rm el} + H_{\rm lat}, \tag{1}$$

where

$$H_{\rm el} = \sum_{m,s} \varepsilon_m c^\dagger_{m,s} c_{m,s} - t_{m,m+1}\left(c^\dagger_{m+1,s} c_{m,s} + \text{H.c.}\right). \tag{2}$$

As usual the transfer integral and the on-site energies are linearized with respect to the in-chain bond length change $v_m = y_{m+1} - y_m$ and the internal coordinate u_m:

$$t_{m,m+1} = t_0 - \gamma v_m, \tag{3}$$

$$\varepsilon_m = (-1)^{m+1}\frac{\Delta\varepsilon}{2} - \frac{[1-(-1)^m]}{2}\alpha u_m. \tag{4}$$

Here $\Delta\varepsilon > 0$ denotes the difference of on-site energies between molecular (A) sites and atomic (B) sites in the undistorted metallic state. Molecular (A) sites are supposed to be odd numbered sites. Finally, treating the lattice degrees of freedom as classical variables, the lattice part of the Hamiltonian reads

$$H_{\rm lat} = \frac{1}{2}\sum_m (M_m \dot{y}_m^2 + \mu_A \dot{u}_m^2 + K_u u_m^2 + K_v v_m^2), \tag{5}$$

where $\mu_A = 0.5 M_{\rm O}$ is the reduced oxygen mass connected with the internal mode, $M_A = 2M_{\rm O} + M_{\rm Cu}$ for $m \in A$ and $M_B = M_{\rm O}$ for $m \in B$. For fixed values of u_m and v_m, an eigenstate of $H_{\rm el}$ is

$$|\mu\rangle = \sum_m \psi_\mu(m) c^\dagger_{m,s} |0\rangle, \tag{6}$$

where the quantum number μ contains the spin index s. In the static approximation the minimum of the total energy (equilibrium structure) is reached if u_m and v_m satisfy the self-consistency equations

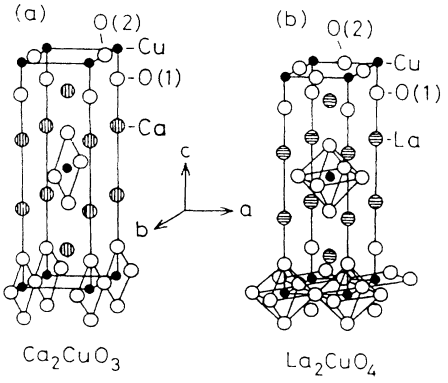

FIG. 2. Crystal structures of Ca_2CuO_3 (a) and La_2CuO_4 (b) [with permission of Yoshida *et al.* (Ref. 9)]. Notice the different notation of oxygens used in the text.

$$u_m = \frac{\alpha}{K_u}(\Lambda_u + P_{m,m}), \qquad v_m = \frac{2\gamma}{K_v}(\Lambda_v - P_{m,m+1}), \tag{7}$$

where

$$P_{m,m'} = \sum_{\mu}^{\text{occ}} \psi_\mu^*(m)\psi_\mu(m'), \quad \Lambda_u = -\frac{2}{N}\sum_{m\in A} P_{m,m},$$

$$\Lambda_v = \frac{1}{N}\sum_m P_{m,m+1}.$$

$P_{m,m'}$ denote the charge and bond order matrix, Na the chain length, and a the Cu-O(1) distance. The Lagrange multipliers Λ_u, Λ_v have been introduced to avoid renormalizations of $t_0 \to t_0 - \gamma\tilde{v}$ (Ref. 1) and $\Delta\varepsilon \to \Delta\varepsilon - \alpha\tilde{u}$ (Refs. 13 and 14) due to constant shifts $\tilde{u}$ and $\tilde{v}$ of u_m, and v_m resulting from the addition of the electrons described by Eq. (2) to the core Hamiltonian and to a lesser extent from the Peierls transition. The CDW-BOW induced period-4 superstructure can be characterized by two equilibrium parameters u_0, v_0:[13,14]

$$u_m = u_0 \sin\left(m\frac{\pi}{2}\right), \qquad v_m = v_0 \cos\left(m\frac{\pi}{2} - \frac{\pi}{4}\right), \tag{8}$$

which depend on the coupling constants

$$\lambda_u = \frac{\alpha^2}{K_u t_0}, \qquad \lambda_v = \frac{\gamma^2}{K_v t_0}, \tag{9}$$

and the electronic heterogeneity parameter $\Delta\varepsilon$.

In order to discuss long-wavelength phonons, we consider small vibrations around the equilibrium values of (u_m, v_m). Within a frozen-phonon-type calculation used here one calculates the total energy in the static approximation at slightly displaced (nonequilibrium) lattice positions to get a second order expansion [the first order terms vanish due to the self-consistency Eqs. (7)]. The electronic part of the total energy,

$$\mathcal{E}_{\text{el}} = 2\sum_k^{\text{occ}} E_k, \qquad \text{with} \quad H_{\text{el}}\psi_k = E_k\psi_k,$$

is obtained readily in the Bloch-wave representation from a 4×4 electronic eigenvalue problem yielding E_k ($-\pi/4 \le ka < \pi/4$).[13,14] Alternatively it can be obtained also from the diagonalization of the periodic chain Hamiltonian with $N \sim 120$–200 sites. It has the calculational advantage of real eigenstates convenient for the determination of matrix elements entering the optical conductivity (absorption) in the random phase approximation,[15]

$$\sigma(\omega) = \frac{\pi}{\omega}\sum_l |\, J_l \,|^2\, \delta(\mathcal{E}_l - \mathcal{E}_0 - \hbar\omega)$$
$$= \frac{\pi}{\omega}\sum_{\alpha,\beta} |\, J_{\alpha\beta} \,|^2\, \delta(E_\alpha - E_\beta - \hbar\omega), \tag{10}$$

where J_l or $J_{\alpha\beta}$ denotes the matrix element of the total current operator,

$$J_l = \langle\Phi_0 \mid \frac{1}{\sqrt{N}}\sum_{n=1}^{N} J(n) \mid \Phi_l\rangle$$
$$= \frac{-2ie}{\sqrt{N}}\sum_{n=1}^{N} t_{n,n+1}[\psi_\alpha(n)\psi_\beta^*(n+1)$$
$$-\psi_\alpha(n+1)\psi_\beta^*(n)],$$

between final (Φ_l) and initial (Φ_0) states with total energies $\mathcal{E}_l$ and $\mathcal{E}_0$, respectively. $E_{\alpha(\beta)}$ and $\psi_{\alpha(\beta)}$ denote the one-particle energies and wave functions of occupied (unoccupied) states [Eq. (6)], respectively. The current operator reads as

$$J(n,s) = -iet_{n,n+1}\left[c_{n,s}^\dagger c_{n+1,s} - c_{n+1,s}^\dagger c_{n,s}\right].$$

The second order derivatives of $\mathcal{E}_{\text{el}}$ with respect to the lattice displacements entering the dynamical matrix D (see below) have been calculated at the minimum of the total energy using the standard finite differences expression.

In the period-4 superstructure we have four longitudinal degrees of freedom, $y_1, \ldots, y_4$, and two internal ones u_1 and u_3 per unit cell, where the subscript denotes the site number. Hence, there will be six modes to be found as the eigenvalues of the 6×6 problem,

$$\| \omega^2\delta_{r,r'} - D_{r,r'} \| = 0, \tag{11}$$

where $D_{r,r'}$ denotes the dynamical matrix which is easily obtained from the classical equations of motion including also electronic Hellmann-Feynman forces. The modes can be classified as symmetric or antisymmetric with respect to a mirror plane (perpendicular to the chain axis) containing the molecule (A) site. According to Fig. 1(b) and to Eq. (8), the same symmetry with respect to B sites is broken by the superstructure. Thus the matrix D can be written as a direct sum of a 3×3 matrix describing the Raman active symmetric modes, a 2×2 matrix describing infrared (ir) active antisymmetric modes, and a 1×1 matrix corresponding to the inactive acoustic mode with $\omega = 0$, which is of no interest.

It is convenient to introduce dimensionless notation $\mathcal{E}_{\text{el}} \to \mathcal{E}_{\text{el}}/t_0$, $\bar{u} \to \alpha\bar{u}/t_0 \equiv \bar{Q}$, $u_m \to \cos(m\pi/2)\alpha u_m/t_0 \equiv Q$, and $v_m \to \sqrt{2}\sin(m\pi/2 - \pi/4)\gamma v_m/t_0 \equiv q$, where $\bar{u}$ describes a small homogeneous transverse deformation of all A sites. The 3×3 "Raman" block reads

$$D_{i,j}^{(3)} = \begin{pmatrix} \frac{2K_v}{M_B}\left(1 + \frac{\lambda_v}{2}\frac{\partial^2\mathcal{E}_{\text{el}}}{\partial q^2}\right) & \sqrt{\frac{\lambda_u K_u \lambda_v K_v}{2\mu_A M_B}}\frac{\partial^2\mathcal{E}_{\text{el}}}{\partial q\partial\bar{Q}} & \sqrt{\frac{\lambda_u K_u \lambda_v K_v}{2\mu_A M_B}}\frac{\partial^2\mathcal{E}_{\text{el}}}{\partial q\partial\bar{Q}} \\ \sqrt{\frac{\lambda_u K_u \lambda_v K_v}{2\mu_A M_B}}\frac{\partial^2\mathcal{E}_{\text{el}}}{\partial q\partial\bar{Q}} & \frac{K_u}{\mu_A}\left(1 + \frac{\lambda_u}{2}\frac{\partial^2\mathcal{E}_{\text{el}}}{\partial Q^2}\right) & \frac{\lambda_u K_u}{2\mu_A}\frac{\partial^2\mathcal{E}_{\text{el}}}{\partial Q\partial\bar{Q}} \\ \sqrt{\frac{\lambda_u K_u \lambda_v K_v}{2\mu_A M_B}}\frac{\partial^2\mathcal{E}_{\text{el}}}{\partial q\partial\bar{Q}} & \frac{\lambda_u K_u}{2\mu_A}\frac{\partial^2\mathcal{E}_{\text{el}}}{\partial Q\partial\bar{Q}} & \frac{K_u}{\mu_A}\left(1 + \frac{\lambda_u}{2}\frac{\partial^2\mathcal{E}_{\text{el}}}{\partial\bar{Q}^2}\right) \end{pmatrix}, \tag{12}$$

and there is an analogous expression for the 2×2 matrix describing the ir active modes:

$$D^{(2)}_{i,j} = \begin{pmatrix} \frac{2K_v}{\mu_{AB}}\left(1 + \frac{\lambda_v}{4}\frac{\partial^2 \mathcal{E}_{el}}{\partial \xi_1^2}\right) & \frac{\lambda_v K_v}{\sqrt{2\mu_{AB} M_A}}\frac{\partial^2 \mathcal{E}_{el}}{\partial \xi_1 \partial \xi_2} \\ \frac{\lambda_v K_v}{\sqrt{2\mu_{AB} M_A}}\frac{\partial^2 \mathcal{E}_{el}}{\partial \xi_1 \partial \xi_2} & \frac{2K_v}{M_A}\left(1 + \frac{\lambda_v}{2}\frac{\partial^2 \mathcal{E}_{el}}{\partial \xi_2^2}\right) \end{pmatrix}. \tag{13}$$

Here the new coordinates ξ_i $(i = 1, 2)$ are related to the displacement y_i at the ith site as follows:

$$\xi_1 = \frac{\gamma}{2t_0}\left(-y_1 + y_2 - y_3 + y_4\right),$$

$$\xi_2 = \frac{\gamma}{\sqrt{2}t_0}\left(y_1 - y_3\right),$$

and $\mu_{AB} = M_A M_B/(M_A + M_B)$ denotes the reduced mass.

It should be noted that the present approach is formally equivalent to a phenomenological, purely elastic, description provided forces up to second-nearest neighbors are taken into account. Hence, phenomenological descriptions restricted to nearest neighbor forces,[3,4] in comparison with a microscopic approach, are approximate only.

The diagonal elements of the dynamical matrix describe a simple renormalization of the bare internal, acoustical, and optical frequencies [two zone-center (ZC) and three zone-boundary (ZB) modes of the undistorted chain]:

$$\omega^b_{\mathrm{int,ZC}} \equiv \omega^b_{\mathrm{int,ZB}} = \sqrt{\frac{K_u}{\mu_A}},\ \omega^b_{\mathrm{opt,ZC}} = \sqrt{\frac{2K_v}{\mu_{AB}}},$$

$$\omega^b_{\mathrm{opt,ZB}} = \sqrt{\frac{2K_v}{M_B}},\ \omega^b_{\mathrm{ac,ZB}} = \sqrt{\frac{2K_v}{M_A}}. \tag{14}$$

The off-diagonal elements describe the mixing of bare modes due to the electron-phonon interaction. All frequencies are softened at least for the parameter sets considered. The softening, especially for the infrared active low-frequency mode, and the mode mixing effects can be quite large. The softening effects should be taken into account if one tries to extract spring constants for effective Hamiltonians from measured phonon modes. Interestingly, the longitudinal mode with the stronger coupling constant is more softened than the weaker coupled internal mode. This is in contrast to the one-component Peierls model where the softening is the stronger the weaker the coupling is (e.g., $\omega \propto \sqrt{\lambda_v}\omega^b_{\mathrm{ac,ZB}}$ for $\lambda_v \ll 1$). It is a consequence of the joint distortion of in-chain displacements and internal degrees of freedom,[13] and it will be investigated in more detail in subsequent work.[14,16]

III. APPLICATION OF THE MODEL TO Ca_2CuO_3

The crystal structure of $Ca_{2-x}Sr_xCuO_3$ shows certain similarities with $YBa_2Cu_3O_7$. In both cases there is a parallel arrangement of CuO_3 chains [in the $y(b)$ direction]. The apical oxygens are sixfold coordinated by divalent cations, by four earthalkalines Ca(Sr) and Ba in the ab plane, as well as by two cations along the $z(c)$ direction, Cu(1) and Ca(Sr) or Cu(2), respectively. The structures of both compounds differ from each other by the absence or presence of anionic metallic $Cu(2)O_2$ planes and a cationic Y plane. The Ca_2CuO_3-type crystal (see Fig. 2) with undistorted chains has an orthorhombic structure with space group $D^{25}_{2h}(I_{mmm})$. By symmetry there are only *two* Raman-allowed modes (having A_g symmetry): one of them connected with displacements of Ca and the other with O(4) diplacements along the z axis. The observed peaks near 306 cm^{-1} and 530–535 cm^{-1} were assigned to these modes. At least three additional peaks in the Raman spectrum, forbidden by the crystal symmetry, near 690 cm^{-1}, 500 cm^{-1}, and 440 cm^{-1} have been observed and should be explained theoretically. As shown below two of them can be explained easily supposing that the ground state of CuO_3 chains is of the CDW-BOW type, leading at least to a doubling of the unit cell in the y direction (in-phase ordering of neighboring chains) and a doubling along the x and z axes, too, for antiphase chain ordering.

A. Parameter choice and mode assignment

Applying Eqs. (1)–(5) to $Ca_{2-x}Sr_xCuO_3$, we adopt a parameter set similar to the sets based on a linear combination of atomic orbitals (LCAO) deformational study we have used recently for the description of CuO_3 chains in $YBa_2Cu_3O_7$.[12] Some changes, e.g., for on-site energies are expected due to the different environment of the chains in both systems: a purely ionic environment for the former and a combination of ionic and metallic environments for the latter. Furthermore, the total charge per chain unit is different as explained in the Appendix. There is an empirical finding that the frequency of the total symmetric Raman mode increases with increasing electronic charge transfer to the CuO_3 chain unit: it comes out about 475–480 cm^{-1} for the insulating $YBa_2Cu_3O_6$ system [having Cu^{1+} ions and isolated $Cu(1)O(4)_2$ molecules instead of CuO_3 chains; the total charge per molecule equals -3], it increases to 500–505 cm^{-1} for $YBa_2Cu_3O_7$ (hereafter denoted as 1-2-3) (Ref. 17) (the total charge of the chain unit $Q_{\mathrm{ch}} \approx -3.5$) and to 524 cm^{-1} for the nonmetallic $PrBa_2Cu_3O_7$ system[18] (the precise value of Q_{ch} is not established yet due to difficulties with the intermediate valency of Pr) and it amounts to 530–535 cm^{-1} for $Ca_{1.8}Sr_{0.2}CuO_3$ (Ref. 9) ($Q_{\mathrm{ch}} = -4$). This increase in the apical oxygen frequencies upon introduction of carriers is a quite general phenomenon which has been observed also for other HTSC's.[17] Thus, the assignment of the 530–535 cm^{-1} mode given in Ref. 9 is in accord with this picture.

According to our calculations in a broad parameter region considered (see below), the aforementioned Raman active mode is only slightly affected by the CDW-BOW induced superstructure. Therefore, the experimentally observed frequency of 530–535 cm^{-1} can be used for a guess of the internal spring constant $K_u = 8.3$–8.5 (7.78 $\mathrm{eV/\AA^2}$ for $YBa_2Cu_3O_7$). The longitudinal spring constant K_v is expected to be larger than in the 1-2-3 system due to the absence of screening metallic cuprate planes.

For the same spring constant K_v as in $YBa_2Cu_3O_7$, K_v =7.57 eV/Å^2, the two "low"-frequency "forbidden" Raman modes could be in principle obtained. The two "high"-frequency "forbidden" Raman modes can be obtained with an enlarged spring constant K_v only. Thus, we examine two values: K_v=18 eV/Å^2 (parameter set I) and 7.57 eV/Å^2 [parameter set II (Refs. 19 and 20)]. In parameter set I the large value of K_v has been obtained fitting the high-frequency infrared mode to the experimentally[9] observed highest-frequency LO phonon at 700–710 cm^{-1}. The remaining parameters for both sets, the coupling constants λ_u= 0.4 (set I), 0.35 (set II) (0.18), λ_v = 0.8(0.85), the electronic heterogeneity $\Delta\varepsilon \approx$ 1.23 eV (set I), 1.33 eV (set II) (1.71 eV), and the transfer integral t_0 =1.4 eV (1.67 eV), are taken near the 1-2-3 values (given in parentheses). The same order of magnitude for coupling constants, the hopping integral, its derivative, and longitudinal lattice distortions has been found in the related MX chains.[1] Calculating the phonon frequencies we have used M_O = 16 a.u. and M_O =18 a.u., respectively. In order to describe approximately a mixture of the ^{63}Cu and ^{65}Cu isotopes found in nature we have adopted an "intermediate" copper mass M_{Cu}=64 a.u.

With parameter sets I (II) one obtains E_g=2.12 eV (2.04 eV), i.e., nearly the experimental gap value (2–2.1 eV), u_0 = 0.15 Å (0.14 Å), and v_0=0.2 Å (0.3 Å) for the internal and longitudinal amplitudes of the superstructure, respectively. Two z positions of the apical oxygen, 0.1–0.13 Å apart from each other, have been observed by extended x-ray-absorption fine-structure (EXAFS) measurements[21] for $YBa_2Cu_3O_7$. Thus, the slightly larger value of 0.14–0.15 Å we predict for Ca_2CuO_3, having the lower commensurability 3/4 compared with 5/8 for 1-2-3, seems to be quite reasonable.

The resulting frequencies are collected and compared to the experimental data in Table I, which contains also the dominant and minor polarization directions. This information derives from the directions and sizes of the atomic and molecular displacements, which are given more quantitatively in Fig. 3. One can observe a substantial mode mixing as a consequence of the electron-phonon coupling. In principle, the mode mixing could be measured by site-selective-isotope substitutions as it becomes possible now for high-T_c superconductors[22] (provided anharmonic corrections can be neglected). Thus, substituting the bridging oxygen or the apical one only, deviations from the standard mass dependence $\omega \propto M_O^{-0.5}$ occur. According to our calculations such effects can be of the order of several percent; see Table II. The total isotope effect, of course, remains unchanged.

For parameter set I two "forbidden" high-frequency ($\geq$ 500 cm^{-1}) Raman modes with the displacement patterns shown in Fig. 3 have been obtained near the experimentally observed values, one of them at slightly lower $\Delta\omega/\omega_{expt}$ = −3% and the other at slightly higher frequency $\Delta\omega/\omega_{expt}$ = 1%. Parameter set II yields the observed "forbidden" modes at lower frequencies with somewhat smaller accuracy +2% (−5%) for the higher (lower) frequency. Hence, we would prefer set I. In the following subsection the polarization properties of the modes obtained with set I are discussed in detail.

TABLE I. Comparison of theoretical and experimental phonon modes. K_u and K_v denote the internal and longitudinal spring constants, and λ_u and λ_v stand for the internal and longitudinal coupling constants, respectively. The dominant (minor) polarization direction is denoted by capitals (small letters) (compare Fig. 3). Modes forbidden by the symmetry of a crystal with undistorted chains are denoted by (*).

K_u (eV/Å^2)	K_v (eV/Å^2)	λ_u	λ_v	ω_{theor} (cm^{-1})	ω_{expt} (cm^{-1})	Polarization activity	
8.5	18	0.4	0.8				
				700	700	Y	ir
				669	690	Y, z	Raman (*)
Parameter set I				530	530	Z, y	Raman
				505	500	Z, y	Raman (*)
				135	?	Y	ir
8.3	7.57	0.35	0.8				
				530	530	Z, y	Raman
				508	500	Z, y	Raman (*)
Parameter set II				455	430	Y	ir
				419	440	Y, z	Raman (*)
				85	?	Y	ir

DISPLACEMENTS OF OPTICAL PHONONS

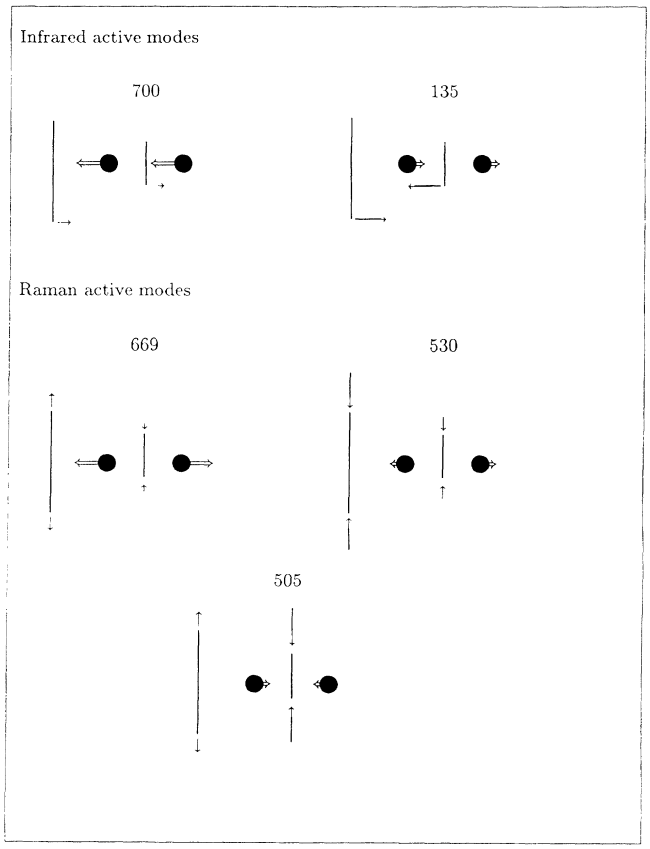

FIG. 3. Atomic and molecular lattice displacements in the optical modes of the two-component alternating chain. Displacements are given for parameter set I of Table I using the same notation as in Fig. 1 for A sites (CuO_2 molecules) and B sites [bridging oxygen O(1)]. The z displacements of the apical oxygens are enhanced by a factor of 2 for better visibility.

B. Mode polarization

First, let us discuss shortly the Raman active modes. The dominant polarization of the calculated 669 cm^{-1} peak is in the y direction with a small admixture of a z-directed component [resulting from the incomplete compensation of the antiphase internal vibrations of neighboring A sites, $A_{z_1} + A_{z_3} = +0.18$ (all atomic displacements involved in Raman active modes are measured in units of the B displacements of this mode)]. This agrees well with the experimentally observed peak near 690 cm^{-1}. The mode at 505 cm^{-1} exhibits the dominant polarization along the z direction and some admixture from y polarization. However, the apical oxygens of neighboring molecules of the 505 cm^{-1} mode move out of phase (the corresponding displacements are -1 for the shortened and 0.35 for the enlarged molecule) in contrast to the in-phase motion for the 530 cm^{-1} mode (-1 for the enlarged and -0.38 for the shortened molecule). The ratio of the squared sum of effective diplacements over the unit cell in the z and y directions, $|A_{z_1}+A_{z_3}|^2/(A_{y_2}+A_{y_4})^2$, yielding a crude estimate of the orientational dependence of the peak intensity, is for the 505 cm^{-1} mode more than 4 times smaller than for the 530 cm^{-1} mode. Experimentally, a weak peak (or a shoulder; see Fig. 4 of Ref. 9) near 500 cm^{-1} has been found for y polarization in the resonance regime [i.e., when the laser frequency (1.96 eV) is near the gap frequency $\approx$ 2 eV]. Unfortunately, in Ref. 9 no figure for the $X(Z,Z)\bar{X}$ scattering configuration in the resonance regime is given. The latter should be compared with the $X(Y,Y)\bar{X}$ spectrum. The 530 cm^{-1} mode in the undistorted metallic chain is polarized along the $z(c)$ direction only, whereas in the CDW phase it gets a small admixture of a component in the chain direction. For off-resonance excitation (laser frequency of 2.54 eV), large intensities polarized in the z direction have been observed as expected. However, weak intensities of polar-

TABLE II. Renormalization of bare phonon modes ω_b [see Eq. (14)] due to the electron-phonon interaction and the partial isotope effects [$^{16}O \rightarrow ^{18}$ O substitutions of bridging oxygen O(1) (B sites) or apical oxygens O(4) (A sites)]. Upper half, parameter set I; lower half, parameter set II. All quantities are given in cm^{-1}.

^{16}O		O(1) substitution		O(4) substitution		Total oxygen substitution	
ω_{theor}	ω_b	ω_{theor}	ω_b	ω_{theor}	ω_b	ω_{theor}	ω_b
135.1	319.4	135.1	319.4	132.4	312.9	132.4	312.9
504.6	537.6	503.8	537.6	476.2	506.9	475.7	506.9
529.8	537.6	529.1	537.6	500.0	506.9	499.5	506.9
668.6	782.4	632.3	737.6	667.3	782.4	630.4	737.6
700.3	845.1	666.6	803.8	698.2	842.6	664.3	801.3
85	207	85	207.1	83.3	202.9	83.3	202.9
418.8	507.4	396	487.4	416.6	507.4	394.8	478.4
454.9	548	433	521.3	453.5	546.5	431.6	519.6
508.3	531.3	507.5	531.3	480.4	500.9	479.2	500.9
530.1	531.3	529.3	531.3	501.1	500.9	499.8	500.9

ization in the x direction have been detected also. This might be caused by a zigzag chain deformation due to out-of-chain displacements [along the $x(a)$ axis] ≈ 0.1 Å of the highly anharmonic bridging oxygens O(1), analogously to its behavior in $YBa_2Cu_3O_7$ observed by high-resolution neutron powder diffraction.[23] Another possibility would be interchain coupling effects, e.g., an out-of-phase ordering of the CDW's at neighboring chains. Such two-dimensional effects are beyond the scope of the present paper.

Turning now to the infrared (ir) active modes, let us note that they are also affected by the mode mixing. It manifests itself in the occurrence of small (0.25) B-site (atomic) displacements and slightly different displacements of out-of-phase moving A sites (e.g., 0.92 for the enlarged molecule against −1 for the shortened one, where the latter diplacement is taken as the unit of all atomic displacements involved in ir modes) in the low-frequency ("descending" from the zone-boundary acoustic mode of the undistorted chain) infrared active mode at 135 cm^{-1} (see Fig. 3). Analogously, the A displacements within the high-frequency infrared active mode (descending from the zone-center mode of the undistorted chain) differ significantly from each other and deviate consequently also from the mass ratio $-M_B/M_A \approx 0.2$ (in units of the B-site displacements). Thereby the shortened (enlarged) molecule with the maximum (minimum) of the CDW [see Fig. 1(c)] shows the smaller (larger) displacements 0.12 (0.22). This differs from results of the phenomenological description of the longitudinal modes of the Pt-Cl chains given in Fig. 3 of Ref. 3, where in the high-frequency infrared active mode the Pt^{IV} sites are much more affected than the Pt^{II} sites.

C. Discussion

The low-frequency infrared active mode calculated at 135 cm^{-1} involves large in-chain displacements of the A sites. Hence, it is probably strongly affected by the interaction of the apical oxygens with Ca ions residing in the same crystallographic (001) plane. Introducing an additional term in Eq. (5) accounting for the hindered motion of the O(4) ions along the chain axis,

$$\frac{K_y}{2}\sum_{m\in A} y_m^2 \quad ,$$

where $K_y \sim$ 10–20 eV/Å^2 denotes the spring constant for the *absolute* longitudinal displacements of the A sites, we get a large increase of this mode. Thus, it could be easily shifted to 260 cm^{-1}, the lowest so far observed LO phonon. However, we should mention that in the frequency region about 200–450 cm^{-1} the CuO_2 molecule can be treated as a rigid object approximately, only.

Some additional hardening required for the 669 cm^{-1} and the 135 cm^{-1} modes can be easily obtained introducing second-nearest neighbor force constants K_v^{AA} and K_v^{BB}. This would be in accord with the long-range nature of Coulomb forces in systems having partially ionic character. The 530 cm^{-1} and the 505 cm^{-1} modes are nearly unaffected by possible second neighbor interactions due to their small y components. As an illustration we refer the reader to the MX chains,[1] where $K^{Pt,Pt} \approx 0.11K^{Pt,Br}$ has been adopted for the second-nearest neighbor (Pt-Pt) force constants to fit the Raman and infrared modes of the PtBr compound whereas the calculated frequencies for the PtCl compound having the strongest electron-lattice interaction were about 20% below the experimental frequencies. No matter how, such problems are beyond the scope of our simple model. They could be discussed quantitatively provided the basic assumption of the present paper, the period-4 CDW-BOW ground state of CuO_3 chains, will be confirmed experimentally. The other electron-lattice interactions of the general Hamiltonian[12] can be treated easily in the same manner as the interactions taken into account above, but additional fit parameters appear. In order to avoid such a situation where the number of predicted modes is reduced we have preferred the approach where the neglected interactions are lumped at least partially in the two effective parameters α and γ of the reduced Hamiltonian, Eqs. (1)–(3). In particular, for fixed γ and v_0 the experimental gap value could be reproduced for $2\sqrt{2}\beta v_0 = \alpha u_0$,[14] yielding an upper limit of $\beta <$1.09 eV/Å, where $\beta = \beta_A = \beta_B$ denotes the intersite diagonal electron-lattice interaction widely used for the MX chains.[1] Adopting the β values of Ref. 1, $\beta \sim$ 0.1–0.2 eV/Å, which are an order of magnitude smaller than this maximal value, we arrive with even larger numbers $\beta \lesssim 0.5$ eV/Å at only slightly changed frequencies. However, at fixed values of α, the β-interaction terms could be helpful to reduce somewhat the large value of γ=4.48 eV/Å towards the estimated value of 3–3.2 eV/Å [see Eq. (A4)].

Finally, the calculation of the frequency-dependent longitudinal optical conductivity (see Fig. 4) has been

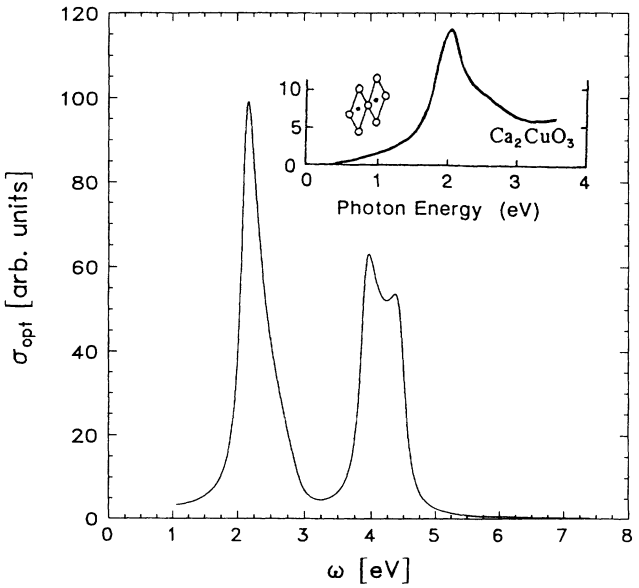

FIG. 4. Optical conductivity σ_{opt} in chain direction vs frequency (for parameter set I; see text and Table I). In the inset the experimental data [Yoshida *et al.* (Ref. 9), in 10^2 Ω^{-1} cm^{-1}] are shown for comparison (with permission from the authors).

performed for a long periodic chain with $N = 120$–200 sites [replacing the δ functions in Eq. (10) by Lorentzian functions to smooth oscillations resulting from discrete level effects caused by the finite chain length]. The optical absorption consists of two strong and one weak absorption bands corresponding to $a \rightarrow a^*$, $b^* \rightarrow a^*$, and $b \rightarrow a^*$ interband transitions, respectively [see Fig. 1(d)]. The first absorption band extents from 2.12 eV until 2.92 eV and the second one from 3.9 eV until 4.47 eV. Comparing the theoretical optical absorption spectrum with the experimental one, qualitative agreement can be found. Quantitative comparison requires structural data as the volume fraction of a chain and the interatomic distances within the chain which were not given in Ref. 9. The calculated optical conductivity clearly exhibits two Van Hove singularities: at the Peierls gap $E_{s1} = 2\Delta_0$, resembling the asymmetric shape of the experimental curve near 2 eV, and at the onset of interband transitions from the second absorption band at $E_{s2} = 0.5\Delta\varepsilon + \mu_F + \Delta_0$=3.9 eV [see Eqs. (A6) and (A7)]. The experimentally observed minimum near 3.2 eV is assigned to the gap between the first and second absorption bands mentioned above. Unfortunately, experimental data of oriented single crystals are available for $\omega \lesssim 3.5$ eV only. In order to check our model it would be interesting to extent the measurements until $\approx$ 5–6 eV since the second peak predicted near 4 eV is sensitive to the value of $\Delta\varepsilon$.[24] The experimentally observed intragap absorption might be caused by the absorption of photoexcited nonlinear excitations as polarexcitons, breathers, etc., vibronic effects,[25] quantum effects such as zero-point motion,[26] by a temperature-dependent pure excitonic effect,[27] or simply by chemical disorder (e.g., random Sr positions or vacancies). Further experimental and theoretical work is required to elucidate its origin. Nonlinear excitations or defect states which break locally the translational symmetry could be responsible also for additional Raman-forbidden lines.

In principle, retaining also nonlinear expansion terms in the on-site energies and hopping integrals within a more detailed description of the molecular A site resulting in a four-band model for the chain (see the Appendix), the infrared active mode associated with the in-phase vibrations of two apical oxygens perpendicular to the chain (in the c direction) can be considered in a generalized Hamiltonian. In the zero-hopping limit [Cu$\rightarrow$ O(1), O(4)$\rightarrow$ O(1)] of this Hamiltonian the chain has either a CDW ground state with total charges of $-5|e|$ and $-3|e|$ of both A sites, respectively, or a ground state with dynamical intramolecular charge fluctuations between Cu and O(4) sites (all A sites with the total charge of $-4|e|$) (Ref. 28) for large quantum corrections tending to a ferroelectric (or an antiferroelectric) ground state for small quantum corrections. For finite values of the transfer integrals mentioned above and a large enough electron-phonon interaction favoring the Peierls transition a coexistence of intramolecular charge fluctuations and a static CDW-BOW in the chain direction is expected. The coupling of the transverse ir mode to, e.g., O(4)-p_z states results in two additional modes having a strong intensity in the ir spectrum and a weak intensity in the Raman spectrum. The magnitude of the splitting of these modes depends on the details of the CDW-BOW state.

IV. CONCLUSIONS AND FINAL REMARKS

The strength of electron-phonon effects in the planar (2D) CuO_2 systems and in the chain (1D) CuO_3 systems is different because the Peierls mechanism in a half-filled 2D band is much weaker in comparison with an 1D one. However, it is commonly believed that correlation effects in many Cu-O systems play important role.[29] For these reasons, probably, the CDW instability in the quasi-two-dimensional La_2CuO_4 system having also a half-filled antibonding Cu-O band is suppressed.

To estimate the effective Coulomb interactions on the chain A and B sites one obtains with help of Eq. (A2)

$$U_{\mathrm{eff},A} = \xi_d^4 U_d + 2\xi_p^4 U_p + 4V_{pd}\xi_d^2\xi_p^2 - V_{AB} \approx \xi_d^4 U_d - V_{AB}, \tag{15}$$

$$U_{\mathrm{eff},B} = U_p - V_{AB}, \qquad V_{AB} = \xi_d^2 V_{pd} + 2\xi_p^2 V_{pp}, \tag{16}$$

where $U_d \approx$ 7–10 eV, $U_p \approx$ 2–4 eV, $V_{pd} \approx 1.2$ eV, and $V_{pp} \approx 0.5$ eV stand for atomic site values. For typical chain values t_0, $\partial\varepsilon_d/\partial u$, $\partial\varepsilon_p^{(4)}/\partial u \lesssim 0.5$ eV/Å, $t_{pd} \approx$ 1.2–1.6 eV, the fitted value of α=2.18 eV/Å can be reproduced provided the electronic heterogeneity at A sites is not too large: $\varepsilon_* \approx 0.7$ [see Eqs. (A3) and (A5)]. In that case from Eqs. (15) and (A2)–(A5) it follows that $\xi_d^2 \approx 0.7$ and we arrive at the values $U_{\mathrm{eff},A} \approx$ 3–4 eV and $U_{\mathrm{eff},B} \approx$ 1–3 eV due to the delocalized character of the molecular antibonding state.

Note that the longitudinal interaction parameter γ is expected to be larger than internal one α due to the reducing factor $s(\varepsilon_*)/\varepsilon_*$ in Eq. (A3). This is in qualitative agreement with the rather large empirical value of 4.48 eV/Å. For $\xi_d^4 \sim 0.5$ an appreciable negative oxygen-oxygen transfer integral $t_{pp} \approx -$(0.4–0.6) eV is required to reproduce the value of the effective transfer integral $t_0 = 1.4$ eV assuming $t_1 \approx$ 1.3–1.4 eV somewhat smaller than $t_{pd} \approx 1.5$ eV. This is in accord with the expected larger values of $a \approx 1.94$ Å in comparison with the intramolecular distance $R_{pd} \approx 1.85$ Å (all distances are estimated by $YBa_2Cu_3O_7$ data).

Comparing now the average mean-field Coulomb energy per site (considering the period-4 CDW-BOW state), W_{Coul}, with the corresponding one-particle electronic energy W_{CDW}, we have found out that both quantities are of nearly the *same* magnitude $W_{\mathrm{Coul}} \approx |W_{\mathrm{CDW}}| \approx 1.6$ eV. Hence, we arrive at a similar interaction regime as in the polyacetylene (PA) case. Since many physical properties of PA have been successfully described within the one-particle SSH model,[38] we expect that the present one-particle approach may be regarded also as a reasonable starting point for more sophisticated investigations.

According to recent polarized x-ray absorption data of Nücker *et al.*[30] for untwinned $YBa_2Cu_3O_7$ there is an appreciable part of oxygen holes with p_z character which means that the corresponding coefficient ξ_p^2 cannot be very small and therefore we arrive again at a somewhat

suppressed value of $\xi_d^2 < 0.7$, pointing to a moderate U_{eff} in agreement with the estimate given above. Furthermore, from Eq. (A2) a relatively small value of $\varepsilon_d - \varepsilon_p^{(4)}$ follows in agreement with the fitted electron-phonon interaction α and Eq. (A3) mentioned above. Hence, there are also experimental hints that the electron-electron correlations in these CuO_3 chains can be weaker than in cuprate planes.

Quite interestingly, Fehrenbacher and Rice[31] have shown that the optical absorption connected with the CuO_3 chains (possibly $\frac{5}{8}$ filled) of the insulating $PrBa_2Cu_3O_7$ compound cannot be described within a one-dimensional t-J model only (as the manifestation of strong correlation effects) but that moderately strong electron-phonon coupling to the internal Raman active mode considered above should be taken into account.

These hints for the non-negligible role of electron-lattice interaction and the fact that the present model Hamiltonian describes well several experimental data lead us to the assumption that in $Ca_{2-x}Sr_xCuO_3$ a period-4 CDW-BOW ground state may survive the intermediately strong electron-electron interaction. Otherwise an antiferromagnetic ground state would be expected.[32,33] However, the observation of magnons as the corresponding collective excitations[34] or that of the upper Hubbard band[30] have been reported so far for two-dimensional cuprates, only.

Regarding the nature of the ground state one should keep in mind that the omitted electron-electron interactions are strongly distant dependent. Thus, on the one hand they are expected to supress the CDW-BOW ground state and to favor magnetic states; on the other hand they give additional sources to the electron-phonon interaction [see, e.g., Eq. (15) in connection with the modulation of ξ_d^4 by the internal mode].

In conclusion, within the present one-particle approach based on optical, ir, and Raman data, the magnitude of the accompanied superstructure has been predicted. Corresponding experimental structural refinements would be highly desirable. A number of other experimental studies, such as site-selective-isotope substitution, extension of the optical conductivity measurements until $\approx$ 5–6 eV, and Raman-scattering spectra of $Ca_{2-x}Sr_xCuO_3$ in a $X(Z,Z)\bar{X}$ configuration in the resonance regime, could also check the main conclusions of the present paper. Doping studies by the substitution of Sr by alkalines (hole doping) or trivalent metals (electron doping) would be of great interest for the study of charged nonlinear excitations as polarons, bipolarons, polarexcitons, and solitons.[12,14] Considerable asymmetric behavior between electron and hole doping is predicted within the framework of these models. Finally, we emphasize that the relative structural simplicity of the $Ca(Sr)_2CuO_3$ compound compared with other metal oxides and MX chain compounds should stimulate further experimental and theoretical studies of this remarkable system. The detailed study of metal-oxygen-bridged chains[32] can be helpful for a better general understanding of the interplay of the electron-lattice interaction and correlation effects and in this context it might contribute also to the elucidation of the high-T_c mechanism itself.

Note added in proof. A further consequence of a CDW at the apical oxygens of neighboring CuO_2 molecules would be the occurrence of two different Ca-O(4) spring constants within a nearest-neighbor three-dimensional approximation for Ca_2CuO_3. Hence, the Ca vibrations are likely affected by the CDW-BOW, too. One might alternatively assign the observed additional "Raman-forbidden" mode near 235 cm^{-1} (below the strong mode near 306 cm^{-1} ascribed to Ca) to a further Ca-vibrational mode instead of to a Cu-vibrational mode as suggested in Ref. 9. The weak shoulder seen near 470 cm^{-1} and a peak near 670–675 cm^{-1} could be interpreted as two-phonon scattering, where in the latter case the 440 cm^{-1} mode is involved.

ACKNOWLEDGMENTS

We thank the SFB 247 at the University of Heidelberg, and the IFW Dresden e.V. for the hospitality of one of us (M.L.) and financial support. The Deutsche Forschungsgemeinschaft is also acknowledged for financial support (S.-L.D. and J.M.) under projects Es-85/1-1 and Dre-269/2-1. Discussions with Professor H. Eschrig, Professor L.S. Cederbaum, Dr. R. Schumann, and Dr. S. Zalis are gratefully acknowledged. The authors are indebted to Professor S. Uchida for stimulating interest and for providing us with experimental data prior to publication.

APPENDIX: ELECTRONIC STRUCTURE OF CuO_3 CHAINS

In this appendix we give some elementary molecular orbital (MO) type remarks on the electronic structure of CuO_3 chains for readers not familar with the electronic structure of Cu-O systems. Supposing that Ca and Sr are fully ionized (+2), i.e., having the electron occupancy [Ar] $4s^0$, [Kr] $5s^0$, respectively, and all oxygens to be (−2), ([Be] $2p^6$) one gets Cu(+2), i.e., a $3d^9 4s^0$ electronic occupancy. Because of the crystal field, the degeneracy of the five Cu $3d$ states is lifted. The highest (nondegenerate) orbital becomes singly occupied. Accounting now for the hybridization between this orbital and doubly occupied $2p_z$ and $2p_y$ orbitals of the apical and the bridging oxygens, respectively, there is some charge redistribution between Cu and O sites, but the highest occupied band remains half-filled.[35]

According to a tight-binding analysis of LDA band-structure calculations for $YBa_2Cu_3O_7$ and to Hückel-type calculations for CuO_4 clusters, the chain band can be constructed approximately as follows. Considering at first a CuO_2 "molecule" with two $2p_z$ orbitals of the O(4) (apical) oxygens with the on-site energy $\varepsilon_p^{(4)}$, the Cu $3d_{z^2-y^2}$ orbital with the on-site energy ε_d, and the transfer integral t_{pd} between them, one gets three states: an antibonding (a) state, a bonding (b) state at

$$E_{a,b} = \frac{\varepsilon_d + \varepsilon_p^{(4)}}{2} \pm \sqrt{\left(\frac{\varepsilon_d - \varepsilon_p^{(4)}}{2}\right)^2 + 2t_{pd}^2}, \qquad \text{(A1)}$$

respectively, and a nonbonding (n) state at $E_n = \varepsilon_p^{(4)}$. The latter two MO orbitals are doubly occupied while the antibonding one is singly occupied. The square of the d(Cu) expansion coefficient in this antibonding orbital reads

$$\xi_d^2 = \left(1 - \frac{1}{2 + \varepsilon_*^2 + \varepsilon_* \sqrt{\varepsilon_*^2 + 2}}\right), \qquad \varepsilon_* = (\varepsilon_d - \varepsilon_p^{(4)})/2t_{pd}, \tag{A2}$$

and the apical oxygen coefficient becomes $\xi_p = -\sqrt{0.5(1 - \xi_d^2)}$. The antibonding MO is thought to hybridize with the p_y orbitals of the bridging oxygen O(1) yielding the one-dimensional two-band complex under consideration. The bonding and nonbonding molecular orbitals are included in the core Hamiltonian. The degree of band filling of this two-band complex is apparently 3/4. Thus ε_A of Eq. (4) stands for E_a and ε_B for $\varepsilon_p^{(1)}$. The diagonal electron-lattice interaction [Eq. (4)] described by α results from the Cu(1)-O(4) overlap $\propto t_{pd} \propto 1/R_{pd}^n$, where $R_{pd} \approx 1.84$ Å and $n = 3$–4, as well as from the change of ε_d and $\varepsilon_p^{(4)}$ due to the changed crystal potential,

$$\alpha \approx \frac{n t_{pd} s(\varepsilon_*)}{\varepsilon_* R_{pd}} + \frac{\partial \varepsilon_p}{\partial u}\left[s(\varepsilon_*) - 1\right] - \frac{\partial \varepsilon_d}{\partial u}\left[s(\varepsilon_*) + 1\right], \tag{A3}$$

where

$$s(x) = \left(1 + 2x^{-2}\right)^{-1/2}.$$

The off-diagonal electron-lattice interaction described by γ [Eq. (3)] results from the modulation of the overlap between the antibonding MO and the p_y orbital of the bridging oxygen with contributions from p_y-$d_{z^2-y^2}$ overlap as well as from p_z-p_y, both being of the same order of magnitude,[12]

$$t_0 = \xi_d t_1 + 2\xi_p t_{pp}, \quad \gamma = -\frac{\partial t_0}{\partial a} \approx \frac{n t_1}{a}(\xi_d + \sqrt{2}\xi_p \tau), \tag{A4}$$

where $\tau = t_{pp}/t_1 \sim -(0.3$–$0.5)$ and t_1 denote the O(4)-O(1) and the Cu(1)-O(1) transfer integrals, respectively, and a is the AB-chain lattice constant with the expected value ≈ 1.92–1.94 Å (all distances are estimated from $YBa_2Cu_3O_7$). Finally, the effective electronic heterogeneity of the chain $\Delta\varepsilon$ can be rewritten in the form

$$\Delta\varepsilon = \varepsilon_p^{(4)} - \varepsilon_p^{(1)} + t_{pd}\varepsilon_* \left[1 + s(\varepsilon_*)^{-1}\right], \tag{A5}$$

convenient to estimate the difference of oxygen on-site energies from experimental data.

The Peierls gap $2\Delta_0$ and its "counterpart" $2\Delta_l$, the gap between the occupied bonding bands [see Fig. 1(d)], arise directly from the superstructure. Assuming the Fermi level μ_F at the center of the Peierls gap, one obtains that $2\Delta_0$ exceeds $2\Delta_l$,

$$\Delta_0^2 = \Delta_l^2 + \frac{\rho}{\mu_F}, \tag{A6}$$

where

$$\epsilon_0 = 0.5\Delta\varepsilon, \qquad \rho = \alpha u_0(\epsilon_0 \alpha u_0 + 2\sqrt{2} t_0 \gamma v_0)$$

have been introduced. The Fermi level μ_F is given by

$$\mu_F = \frac{2}{\sqrt{3}}\mu_0 \cos\left(\frac{1}{3}\arccos\left[\frac{3\sqrt{3}\rho}{4\mu_0^3}\right]\right), \tag{A7}$$

where

$$\mu_0 = \sqrt{\epsilon_0^2 + 2t_0^2 + (\gamma v_0)^2 + 0.5(\alpha u_0)^2 - \Delta_0^2}.$$

Finally, we collect some approximate analytic expressions valid in the case of a predominant in-chain electron-phonon interaction and both moderate internal phonon coupling and electronic heterogeneity $\Delta\varepsilon \lesssim t_0$.

The middle gap $2\Delta_m$,

$$2\Delta_m \approx \Delta\varepsilon - \frac{\sqrt{2}\alpha u_0 \gamma v_0}{t_0}, \tag{A8}$$

stems mainly from the electronic heterogeneity between A and B sites. For $\lambda_u \to 0$ the Peierls gap can be estimated as

$$2\Delta_0 = \frac{2\sqrt{2} t_0 \gamma v_0}{\sqrt{\epsilon_0^2 + 2t_0^2}}, \tag{A9}$$

and the total bandwidth W becomes

$$W = 4t_0\sqrt{1 + \left(\frac{\gamma v_0}{t_0}\right)^2 + \left(\frac{\epsilon_0}{2t_0}\right)^2}. \tag{A10}$$

†On leave from Institute of Inorganic Chemistry, 630090 Novosibirsk, Russia.

[1] J.T. Gamel, A. Saxena, I. Batistic', and A.R. Bishop, Phys. Rev. B **45**, 6408 (1992).
[2] I. Batistic' and A.R. Bishop, Phys. Rev. B **45**, 5282 (1992).
[3] A. Bulou, R.J. Donohoe, and B.I. Swanson, J. Phys. C **3**, 1709 (1991).
[4] L. Degiorgi, P. Wachter, M. Haruki, and S. Kurita, Phys. Rev. B **40**, 3285 (1989); **42**, 4341 (1990).
[5] M. Alouani, R.C. Albers, J.M. Wills, and M. Springborg, Phys. Rev. Lett. **69**, 3104 (1992).
[6] M.J. Rice, Phys. Rev. Lett. **37**, 36 (1976).
[7] B. Horovitz, Solid State Commun. **41**, 729 (1982); for further references see E. Ehrenfreund, Z. Vardeny, O. Brafman, and B. Horovitz, Phys. Rev. B **36**, 1535 (1987).
[8] M.J. Rice and E.J. Mele, Phys. Rev. Lett. **49**, 1455 (1982).
[9] M. Yoshida, S. Tajima, N. Kozhizuka, S. Tanaka, S. Uchida, and S. Ishibashi, Phys. Rev. B **44**, 11997 (1991); Y. Tokura, S. Koshihara, T. Arima, H. Takagi, S. Ishibashi, T. Ido, and S. Uchida, Phys. Rev. B **41**, 11657 (1990).
[10] O.K. Anderson, A.I. Liechtenstein, O. Rodriguez, I.I. Mazin, O. Jepsen, V.P. Antropov, O. Gunnarson, and S.

Golopan, Physica C **185-189**, 147 (1991); M. Hirao, T. Uda, and Y. Murayama, *ibid.* **195**, 230 (1992).

[11]Recent studies (Ref. 5) of the electronic structure of $Pt_2Br_6NH_4$ chains, a member of the MX family, have demonstrated first the importance of ligand states for the period-4 superstructure, but the consequences for the transverse electron-lattice interaction have not been considered in detail, yet.

[12]S.-L. Drechsler, J. Malek, and H. Eschrig, Synth. Met. **55-57**, 4626 (1993); H. Eschrig, S.-L. Drechsler, and J. Malek, Physica C **185-189**, 1461 (1991).

[13]F. Fischer, H. Köppel, and L.S. Cederbaum, Z. Phys. B **74**, 513 (1989); Synth. Met. **41-43**, 3597 (1991); (unpublished).

[14]S.-L. Drechsler, J. Malek, H. Köppel, H. Eschrig, and L.S. Cederbaum, Synth. Met. **55-57**, 4272 (1993); J. Phys. IV (France) C2, **3**, 273 (1993).

[15]S.R. Phillpot, A.R. Bishop, and B. Horovitz, Phys. Rev. B **40**, 1839 (1989); S.R. Phillpot, M.J. Rice, A.R. Bishop, and D.K. Campbell, *ibid.* **36**, 1735 (1986).

[16]M. Lavrentiev, H. Köppel, and L.S. Cederbaum (unpublished).

[17]D. Mihailovic, C.M. Foster, K.F. Voss, T. Mertelj, I. Poberaj, and N. Herron, Phys. Rev. B **44**, 237 (1991).

[18]J. Humlicek, A.P. Litvinchuk, W. Kress, B. Lederle, C. Thomsen, M. Cardona, H.-U. Habermeier, I.E. Trovimov, and W. König, Physica C **206**, 345 (1993).

[19]B. Renker, F. Gompf, E. Gehring, G. Roth, W. Reichardt, D. Ewert, H. Ritschel, and H. Mutka, Z. Phys. B **71**, 437 (1988); B. Renker, F. Gompf, E. Gehring, D. Ewert, H. Ritschel, and A. Dianoux, *ibid.* **73**, 309 (1988).

[20]The smaller spring constant $K_v \approx 4.37$ eV/Å^2 we have used (Ref. 12) for the description of $YBa_2Cu_3O_7$ has been deduced from an early shell-model analysis of inelastic neutron data (see Figs. 3 and 4 of Ref. 19) assigning vibrations around 400 cm^{-1} to O(1). However, the later improved shell-model parameter set (Ref. 18) based on more precise Raman and ir data suggests a somewhat larger value 573 cm^{-1} of the infrared active chain mode involving O(1). This mode can be approximately described within our model using K_v =7.57 eV/Å^2 which yields 548 cm^{-1}.

[21]J. Mustre de Leon, S.D. Conradson, and A.R. Bishop, Phys. Rev. Lett. **65**, 1678 (1990); J. Mustre de Leon, S.D. Conradson, I. Batistic, and A.R. Bishop, Phys. Rev. B **44**, 2422 (1991); E.A. Stern, M. Qian, Y. Yacoby, S.M. Heald, and H. Maeda, Physica C **209**, 331 (1993).

[22]D.E. Morris, A.G. Markelz, J.Y. Wei, C.T. Hultgren, J.H. Nickel, J.C. Hamilton, and K.F. McCarty, Phys. Rev. B **44**, 9556 (1991).

[23]M. Francois, A. Junod, J.J. Capponi, P. Strobel, M. Marezio, and P. Fischer, Solid State Commun. **66**, 1117 (1988).

[24]We have learned from extended optical data of Uchida *et al.* (unpublished) that there are indeed two narrow peaks near 4 eV and 4.7 eV in their reflectivity data of pure Ca_2CuO_3 and a 1.5 eV broad peak near 4 eV of $Ca_{2-x}Sr_xCuO_2$. They are expected to cause a second peak in the vicinity of 4 eV (possibly with a weak double peak structure) in the optical conductivity. Quite similarly, the data of Kelly *et al.* [Fig. 7(c) of Ref. 36] on polycrystalline Sr_2CuO_3 show in the imaginary part of the dielectric function a pronounced shoulder near 3.8 eV and two sharp peaks near 4.35 eV and 5.05 eV, respectively. We agree with the suggestions of the authors that the feature near 4.35 eV might be associated with pairs of oxygen vacancies [O(1) in our notation] interrupting the chains and leading to isolated twofold coordinated Cu(1+) ions for which a Cu $3d \rightarrow 4p$ transition near 4.1 eV is well known (Refs. 36 and 37). The analogous transition in the regular chain is expected to be modified due to hybridization with oxygen O(1)-p states and it might be therefore responsible for the somewhat broader peak near 5.05 eV. The pronounced shoulder near 3.8 eV we ascribe to the onset of the interband transition obtained in our fit near 3.9 eV since in the data of Uchida *et al.* for oriented Ca_2CuO_3 the reflectivity perpendicular to the chain direction remains nearly constant.

[25]D. Moses, A. Feldblum, E. Ehrenfreund, A.J. Heeger, T.-C. Chung, and A.G. MacDiarmid, Phys. Rev. B **26**, 3361 (1983).

[26]R.H. McKenzie and J.W. Wilkins, Phys. Rev. Lett. **69**, 1084 (1992).

[27]K. Iwano and K. Nasu, J. Phys. Soc. Jpn. **61**, 1380 (1992).

[28]J. Batistic, A.R. Bishop, R. Martin, and Z. Tesanovic, Phys. Rev. B **40**, 6896 (1989).

[29]A.M. Oles and W. Grzelka, Phys. Rev. B **44**, 9531 (1991).

[30]N. Nücker *et al.*, Europhys. Conf. Abstr. **17A**, 1038 (1993); (unpublished).

[31]R. Fehrenbacher and T.M. Rice (unpublished).

[32]The recently investigated compound $CuGeO_3$ having a similar chemical formula as the Ca_2CuO_3 contains also Cu^{2+} ions but within a CuO_4 chain. The observed spin-Peierls transition [see M. Hase *et al.*, Phys. Rev. Lett. **70**, 3651 (1993)] points to an extremely strong electron-electron correlation $U_{\rm eff} \gg 4t_{\rm eff}$. Its origin results from the bridging by *two off-chain axis oxygens* leading, for geometrical reasons, to a very small effective transfer integral. Furthermore, the two apical oxygens attached the Cu ion are at large distances (2.77 Å) and the hybridization between $3d$ and $2p$ orbitals is strongly reduced. As a result we arrive at $U_{\rm eff} \approx U_d$.

[33]A quite interesting new spin-Peierls state involving $MX(AB)$ pairs *and* large lattice distortions has been found for the strong diagonal intersite electron-phonon interaction β^2/K_v, $\beta_A = -\beta_B$, and Coulomb interaction U: H. Röder, A.R. Bishop, and J.T. Gamel, Phys. Rev. Lett. **70**, 3498 (1993). However, for $t_0 = 0.25\Delta\varepsilon$ and $2U/\Delta\varepsilon < 5$ the period-4 CDW-BOW state exhibits the lowest total energy. In connection with the problem of the behavior of large-U systems near a phase boundary between magnetic and nonmagnetic states, the example of $[Ni(chxn)_2Cl]Cl_2$ [M. Yamashita *et al.*, Synth. Met. **55-57**, 3461 (1993)] is very instructive. The substitution of two Cl^- counter ions by two $[ClO_4]^-$ counter ions converted the MX chain from the Mott-Hubbard state into the same CDW-BOW state as proposed here for Ca_2CuO_3.

[34]M. Yoshida, S. Tajima, N. Koshizuka, S. Tanaka, S. Uchida, and T. Itoh, Phys. Rev. B **46**, 6505 (1992).

[35]In the HTSC compound $YBa_2Cu_3O_7$ the total charge per plane CuO_2 unit is $-(2-\nu)$ and for the chain unit CuO_3 it is $-(3+2\nu)$. The experimental value (e.g., derived from Hall data) of $\nu \approx 0.25$ is in qualitative agreement with LDA band-structure results.

[36]M. Kelly, P. Barboux, J. Tarascon, and D. Aspnes, Phys. Rev. B **40**, 6797 (1989).

[37]J. Kircher, M. Alouani, M. Garriga, P. Murugaraja, J. Maier, C. Thompson, M. Cardona, O. Anderson, and O. Jepsen, Phys. Rev. B **40**, 7368 (1989).

[38]W. Su, J. Schrieffer, and A. Heeger, Phys. Rev. B **22**, 2099 (1980).